# Finite element method analysis of flow and heat transfer of aging heat furnace for aluminum alloy plates

Yelda VELI[1], Marin PETRE[2], Alexandru M. MOREGA*,[1,3], Alin A. DOBRE[1], Alexandra Valerica NECOLA[2]

*Corresponding author
[1]POLITEHNICA University of Bucharest,
Splaiul Independentei 313, 060042, Bucharest, Romania,
yelda.veli@upb.ro, alexandru.morega@upb.ro*, alin.dobre@upb.ro
[2]Vimetco ALRO,
Str. Pitesti 116, 230048, Slatina, Romania,
mapetre@alro.ro, aachim@alro.ro
[3]"Gheorghe Mihoc – Caius Iacob" Institute of Mathematical Statistics and Applied Mathematics of the Romanian Academy,
Calea 13 Septembrie no. 13, 050711 Bucharest, Romania

DOI: 10.13111/2066-8201.2022.14.1.18

*Received: 14 December 2021/ Accepted: 04 February 2022/ Published: March 2022*


***Abstract:*** *Due to its high hardness and easy processing in certain tempers, the 2014 aluminum alloy is often used in the aerospace industry. Therefore, heat treatment for the aging of the 2014 aluminum alloy plates is an important quality concern, and its prediction using numerical simulations may contribute to the optimization of the process. The simulation of the aging treatment covers steps from the introduction of the plates in the furnace, at room temperature until their removal, respectively after 9 hours at 177°C ± 3°C. The simulation results are compared with the industrial tests on an indirectly heated, fuel-fired batch furnace. The study is aimed to determine the airflow inside the furnace and the minimum time to reach the set temperature. The simulation results help to better understand the healing process and to predict the minimum time required for a batch to reach the set temperature according to its weight.*

***Key Words:*** *aging heat treatment, heat furnace, aluminum alloy plates, turbulent heat transfer, numerical simulation, finite element method*

## 1. INTRODUCTION

Precipitation hardening alloys include 2,000, 6,000, and 7,000 series aluminum alloys. After heat treatment and quenching, these alloys can be tempered by heating. The heating treatment at room temperature for several days is called *natural aging*, whereas the treatment at elevated temperatures, usually in the range of 150 to 200°C, is called *artificial aging* [1].

Different types of furnaces were designed by different manufacturers to carry out the aging heat treatment of aluminum alloy plates. All manufacturers pursue the same goal, to design and make furnaces with improved energy efficiency while being as environmentally

friendly as possible. In recent decades, there was an improvement in the design of traditional furnaces along with an important increase in their automatic control.

In all of these processes, an important role is played by mathematical modeling, which is supported by the improvement in numerical methods and the increase of computing power [2]. The most used method for the classification of furnaces is by the mode of operation (either batch or continuous), the method of heating (either directly fired or indirectly heated), and by the type of energy that is used (either fuel-fired or electrically heated) [3].

A model was developed for a Danieli batch treatment furnace with 70 tons maximum load, indirectly heated, fuel-fired for aluminum alloy plates aging treatment (Fig. 1) [4]. The furnace was commissioned in 2019 in the ALRO plant in Romania and is provided with last improvements in temperature control, ensuring the temperature uniformity for the workspace of ± 3°C, in the range of 80°C – 250°C.


Fig. 1 The independent equipment for the research of aluminum alloy plate aging treatment

The model used in the numerical simulation can be divided into three major parts: temperature prediction, phase transformation, and mechanical behavior [4]. In this paper, we focus on studying the steady-state heat transfer and airflow inside the empty and loaded furnace, respectively.

For this analysis, to reduce the numerical complexity and the pending computational load, without losing the main heat transfer characteristics of the process, representative middle and an end part (cells) of the furnace are defined and analyzed.

In most of the published works [5] the heat transfer and the flow for the loaded furnace are studied, but very few works also study the empty furnace, which represents the starting point. In general, the works concerning empty furnaces are those for the treatment of steel [6–8]. In this work, the forced convection heat transfer during the stationary aging temperature of the aluminum batch aging is studied.

Tests and measurements were made to validate the numerical simulation results, including the temperature uniformity survey (TUS) test [9].

Once the model has been obtained, various simulations can be made to optimize the aging process by loading the furnace and simulating the variation of the batch volume, the dimensions of the plates, and their positioning inside the furnace.

## 2. THE MATHEMATICAL MODEL

The heat transfer inside the aging furnace combines all modes of heat transfer: conduction (all over), convection (within the airstream flow), and radiation (between corresponding surfaces). Radiation heat transfer is not accounted for in this study, and it is the object of future work. It is presumed that this assumption may result in a certain discrepancy in the power level that may be needed to reach the specified temperature profile inside the furnace.

The steady-state forced convection heat transfer within the furnace conveyed by an air stream is decoupled, and the two parts – the hydrodynamic flow, and the energy balance – are considered and solved sequentially: first, the airflow and next, to the heat transfer. The thermal properties of air are evaluated at the bulk, working temperature of the batch and there is no mixed (natural and forced) convection heat transfer.

The momentum conservation and mass conservation laws, further formulated for a viscous, present the hydrodynamic part of the problem using a *k-ω* model [10,11]. This two-equation turbulence model is used as an approximation for the Reynolds-averaged Navier-Stokes equations (RANS equations) and it solves for two variables: $k$ [J/m$^3$], the turbulence kinetic energy, and $\omega$ [m$^2$/s$^3$], the specific rate of dissipation of kinetic energy (turbulence frequency). Unlike the *k-ε* models [12,13] – that, instead of $\omega$, accounts for $\varepsilon$, the rate of dissipation of turbulence kinetic energy – which work**s** well for problems of external flow around complex geometries, but less so in cases of large adverse pressure gradients [10], the *k-ω* model is useful in cases such as internal flows, flows that exhibit strong curvature, separated flows, and jets. Under these assumptions the mathematical model for stationary flow is made of:

*momentum balance*

$$\rho(\boldsymbol{u}\cdot\nabla)\boldsymbol{u} = \nabla\cdot\left[-p\boldsymbol{I} + \left(\eta+\eta_T\right)\left(\nabla\boldsymbol{u} + (\nabla\boldsymbol{u})^{\mathrm{T}} - \frac{2}{3}\rho k\boldsymbol{I}\right) - \nabla\cdot\left[\frac{2}{3}\left(\eta+\eta_T\right)(\nabla\cdot\boldsymbol{u})\boldsymbol{I}\right]\right], \tag{1}$$

where the last term in eq. (1), $\nabla\cdot\left[\frac{2}{3}\left(\eta+\eta_T\right)(\nabla\cdot\boldsymbol{u})\boldsymbol{I}\right]$, is enabled only for Ma <0.3.

*RANS equation for the turbulence kinetic energy balance*

$$(\rho\boldsymbol{u}\cdot\nabla)k = P - \beta^*\rho k\omega + \nabla\cdot[(\eta+\sigma_{\mathrm{k}}\,\rho k/\omega)\nabla k], \tag{2}$$

*RANS equation for the specific rate of dissipation of kinetic energy balance*

$$(\rho\boldsymbol{u}\cdot\nabla)\omega = \frac{\alpha\omega}{k}P - \beta\rho\omega^2 + \nabla\cdot[(\eta+\sigma_{\omega}\,\rho k/\omega)\nabla\omega], \tag{3}$$

*mass balance*

$$(\nabla\cdot\rho\boldsymbol{u}) = 0 \text{ for compressible flow, and , } \rho\nabla\cdot\boldsymbol{u} = 0, \text{for incompressible flow.} \tag{4}$$

Here $\boldsymbol{u}$ [m/s$^2$] is the velocity, $p$ [N/m$^2$] the pressure, $\rho$ [kg/m$^3$] the mass density, $\nu$ [s$^{-1}$] the dynamic viscosity, $\boldsymbol{I}$ the unity matrix, $P(\boldsymbol{u}) = (\rho k/\omega)\left[\nabla\boldsymbol{u}\colon(\nabla\boldsymbol{u} + (\nabla\boldsymbol{u})^T) - \frac{2}{3}(\nabla\cdot\boldsymbol{u})^2\right] - \frac{2}{3}\rho k\nabla\cdot\boldsymbol{u}$, Ma = $|\boldsymbol{u}|/a_{\mathrm{air}}$ is the local Mach number, and $a_{\mathrm{air}}$ is the velocity of the sound in the air. The eddy viscosity required by the RANS equations is $\nu_T = k/\omega$. The recommended values for the different parameters are available, *e.g.*, in [11].

The thermal fluid (air) here is presumed Newtonian, and its hydrodynamic and thermal properties are assumed constant and evaluated at the bulk temperature of the stream – it is assumed that the adiabatic mixing of the fluid results in a certain equilibrium temperature that accurately presents the average temperature of the moving fluid, rather than an uncomplicated

average like the film temperature.

The stationary form of the energy equation [14]

$$\rho c(\boldsymbol{u} \cdot \nabla)T = \nabla \cdot (k\nabla T), \tag{5}$$

where $c$ [J/kg·K] is the specific heat and $k$ [W/m$^2$K] the thermal conductivity, is used to model the heat transfer part of the problem.

The convection term in eq. (5) is annulled within the solid parts and copies the result of the hydrodynamic part (the velocity field) within the fluid space. The boundary conditions that close the mathematical model formulated for the CAD computational domain shown in Fig. 2 (the parts are labeled in black) are as follows:

- for the airflow inside the cell (in blue): inlet velocity for the fan outlet, no-slip conditions for the solid walls and slip conditions for the symmetry planes, and uniform pressure for the fan inlet (the airflow inside the fan is not modeled here);
- for the forced convection heat transfer inside the cell (in red): convection heat transfer for the outer surfaces, bathed by air (the top and sidewalls of the furnace); insulation for the symmetry planes, and constant temperature for the bottom.

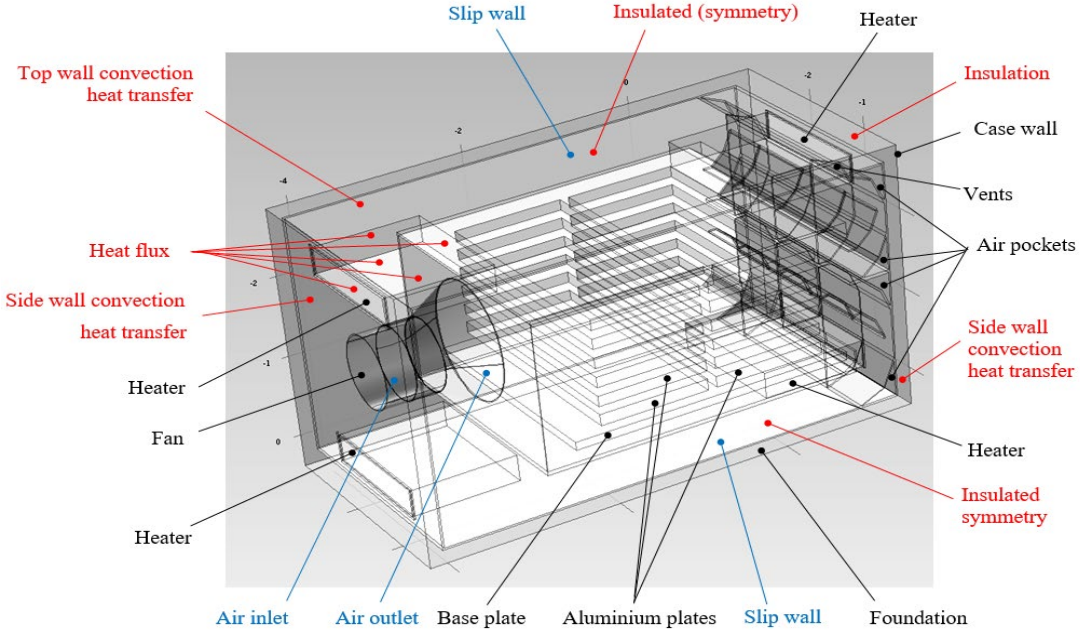


Fig. 2 – The computational domain and the boundary conditions for the loaded furnace, middle cell. Dimensions are in meters

The same boundary conditions are applied to the furnace side cell, except for its end solid (external) wall where no-slip flow condition is set for the inside face of the wall bathed by the air and convection heat transfer to the ambient for the face of the wall exposed to the environment.

The mathematical model (1)-(5) is then solved numerically using the finite element method (FEM).

The main purpose of this numerical simulation endeavor is to find the temperature distribution inside the furnace.

## 3. NUMERICAL SIMULATION RESULTS AND DISCUSSIONS

The numerical simulations envisage the two modules (Fig. 1). The first one is defined assuming geometric and heat transfer symmetry and it is aimed to represent a middle section of the furnace. The second one models the end section of the furnace, which is found at its margins. The mathematical models (flow and heat transfer) are solved sequentially, first the hydrodynamic problem, (1)-(4) and then the energy equation (5).

A difficulty that is encountered in mathematical modeling when using asymptotic like models such as (1)-(3) is that depending on the local flow rate driven by the fan, parts of the air stream flow may be either above or below the local Ma threshold, which either enables or zeroes the last term in the r.h.s. of eq. (1). This condition is difficult (if currently possible) to assert and implement. In the absence of a transition model that may accommodate the two forms of the momentum balance, we consider that the flow regime, which is set through the inlet velocity boundary conditions, is compressible. It is then left for an *a posteriori* inspection of the local Ma number, obtained through numerical simulation, to evaluate and ascertain the validity of this assumption. In other words, this way, the low Ma term in eq. (1) would cancel by calculation rather than arbitrarily discarded.

The compressible, turbulent, stationary airflow is represented in Fig. 3 through arrows and velocity tube lines, whose size and color are proportional to the local flow rate.

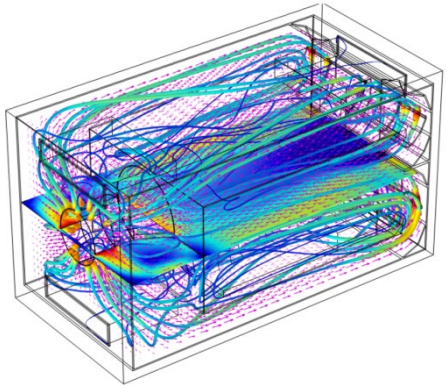

a. Empty furnace, middle cell; $U_{max}$ = ~10 m/s

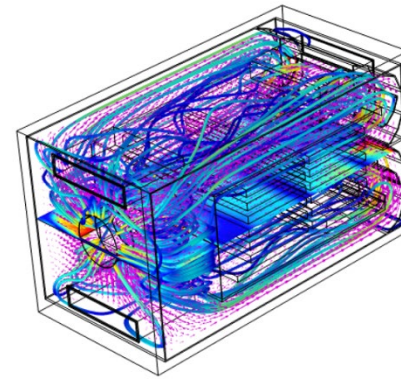

b. Loaded furnace, middle cell; $U_{max}$ = ~15 m/s

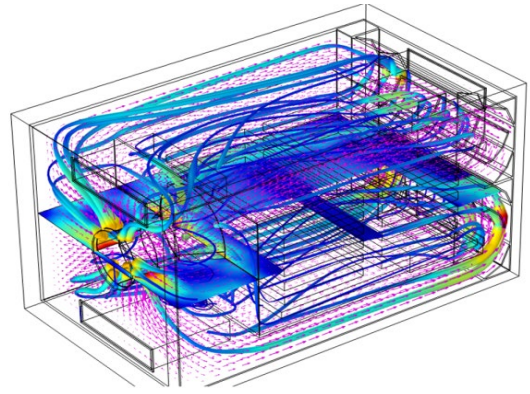

c. Loaded end cell; $U_{max}$ = ~20 m/s

Fig. 3 – The airflow inside the furnace for $U_{in}$ = 10 m/s, $U_{in}$ = 15 m/s and $U_{in}$ = 20 m/s, respectively

The complex structure of the airflow includes both regions of laminar flow – *e.g.*, the spacing between the aluminum alloy plates, when the load is present – as well as complex recirculation regions. The local airflow rates are higher in the spacing between the aluminum alloy plates for the loaded furnace in both middle and end cells. The validation of the compressible flow hypothesis can be performed by representing the distribution of the local Ma number, see Fig. 4. The maximum value of the local Ma number does not exceed the compressible flow hypothesis threshold, $Ma_{max} = \sim 0.032 << 0.3$. The incompressibility of the flow is thus verified *a posteriori*.

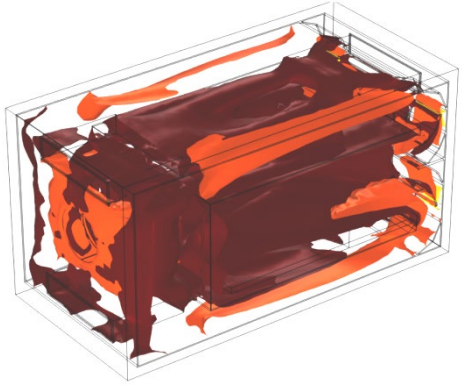

a. Middle cell, empty furnace; local $Ma_{max} = \sim 0.043$, and $U_{in} = 10$ m/s

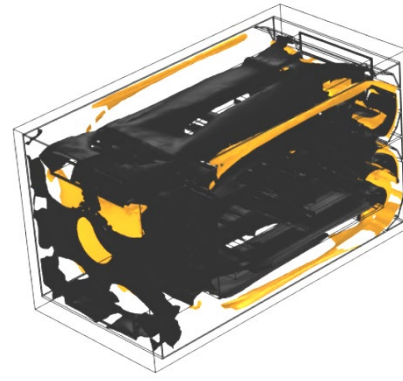

b. Middle cell, loaded furnace; local $Ma_{max} = \sim 0.032$, and $U_{in} = 15$ m/s

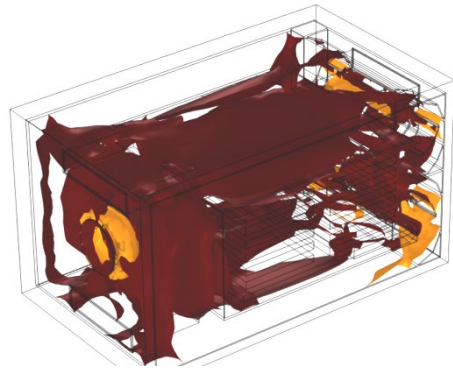

c. Side cell, loaded furnace; local $Ma_{max} = \sim 0.06$, and $U_{in} = 20$ m/s

Fig. 4 – Surfaces of constant Ma (light color indicates higher Ma) for the middle and end cells, respectively.

Reynolds dimensionless group

$$Re_D = Ud/\nu, \tag{6}$$

where $U$ is the flow velocity, $d$ is the pipe diameter, and $\nu$ is the kinematic viscosity of the fluid is commonly used to investigate the pipe flows. However, Re applies to any flow, with "characteristic" flow velocity, $U$, and flow (space) scales, $d$.

The threshold for the Reynolds number, $Re_{D,cr}$, above which the flow becomes unstable and turbulent, is experimentally determined to be between 11,800 and 14,300, but this value is overestimated and justified by using very smooth inlet surfaces for the conducted experiments [15]. Other experimental results set $Re_{D,cr} \approx 2{,}000$. Moreover, in other papers – especially studies using very smooth pipes [16] – laminar flow has been recorded for Reynolds

numbers up to 100,000 [15]. Consequently, the laminar flow region cannot be limited to Reynolds numbers up to 2,000. The roughness of the wall and the inlet conditions can induce turbulences or instabilities, and the flow does not restore to its laminar flow regime if the Reynolds number is high enough: typically, $Re_{D,cr} \approx 2{,}300$ for a cylindrical, circular, straight pipe.

There exists then a critical Reynolds number, $Re_{cr}$, above which the flow becomes unstable and turbulent. This criterion may be used to ascertain the type o flow. Here we are concerned with the *local*, Reynolds cell number $Re_{cell}$ (the flow characteristic dimension is the size of the finite element), whose distribution is depicted in Fig. 5 through surfaces of constant $Re_{cell}$.

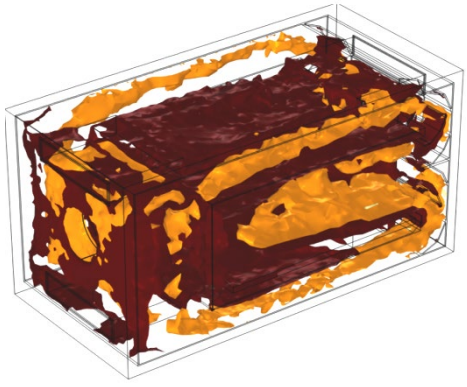

a. Empty furnace, middle cell; $Re_{cell,max} = \sim 1 \cdot 10^2$

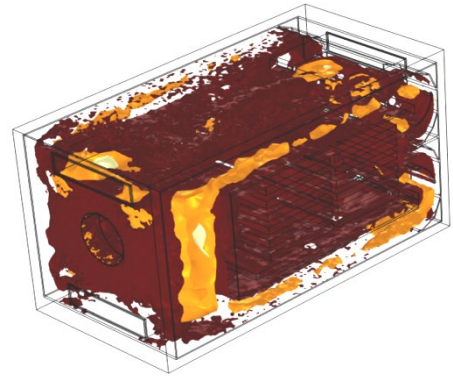

b. Loaded furnace, middle cell; $Re_{cell,max} = \sim 90 \cdot 10^2$

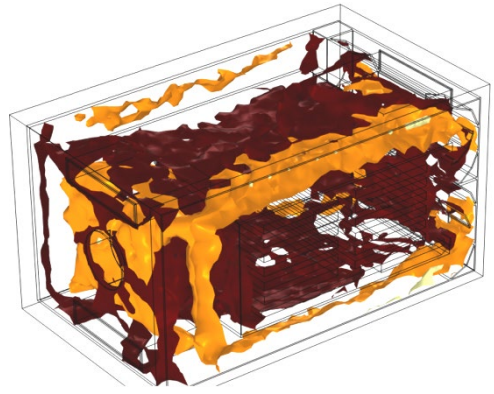

c. Loaded furnace, end cell; $Re_{cell,max} = \sim 170 \cdot 10^2$

Fig. 5 – Surfaces of constant Reynolds cell number (light color) for the empty and loaded furnace – light color indicates higher $Re_{cell}$

The numerical simulation results shown in Fig. 5 suggest that, based on $Re_{cell}$, the flow is turbulent, as presumed. In what concerns the forced convection heat transfer, the Péclet group is relevant:

$$\mathrm{Pe}_D = \frac{Ud}{D} = \mathrm{Re}_D \mathrm{Pr} = \frac{convection\ \text{transport rate}}{\text{diffusive transport rate}} = \frac{diffusion\ time}{\text{convection}\ time}, \tag{7}$$

where $D$ is the thermal diffusivity of the fluid, $\mathrm{Pr} = \nu/D$ is Prandtl group. The Péclet number is analog to the Reynolds number by considering the importance of the convective and diffusive flux. We are concerned here with the cell Péclet number, $Pe_{cell}$.

For the middle cell, empty furnace, the maximum value of the local Péclet cell number is $Pe_{cell,max} \sim 3.5 \cdot 10^{10}$, and for the loaded middle furnace, local $Pe_{cell,max} \sim 3.4 \cdot 10^{4}$. The loaded end cell presents an intermediate value with local $Pe_{cell,max} \sim 7 \cdot 10^{6}$. These results are consistent with the forced convection in a turbulent flow.

The temperature distribution is presented in Fig. 6, and it shows a steep drop in temperature at the furnace walls unlike the uniform temperature distribution seen inside the furnace and within the load package (the aluminum alloy plates).

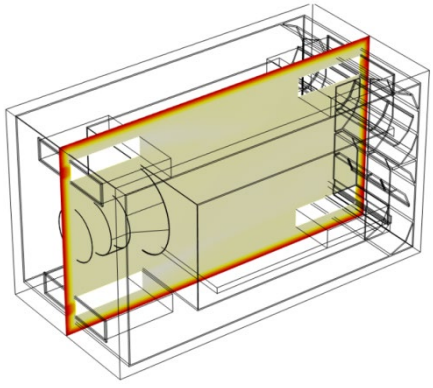

a. Empty furnace, middle cell; $T_{max}$ ~115 °C, $T_{min}$ ~31 °C, $U_{in}$ = 10 m/s

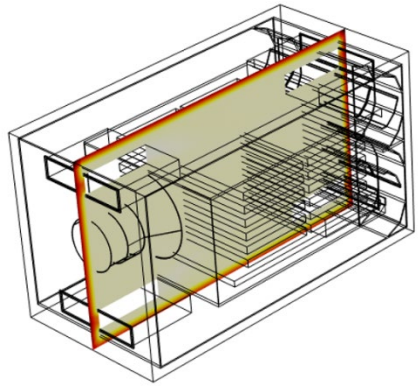

b. Loaded furnace, middle cell; $T_{max}$ ~60 °C, $T_{min}$ ~36 °C, $U_{in}$ = 15 m/s

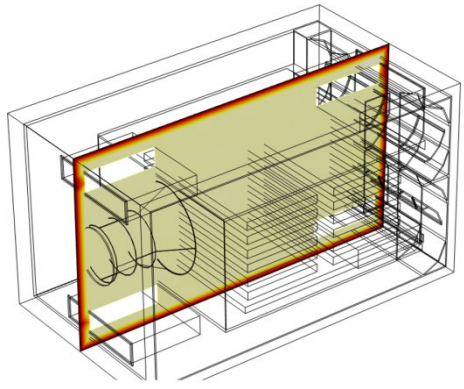

c. Loaded furnace, end cell; $T_{max}$ = ~85 °C, $T_{min}$ = ~34 °C, $U_{in}$ = 20 m/s

Fig. 6 – Cross-section temperature distribution for the empty and loaded furnace

As expected, the temperature distribution and variation do not change for the empty and loaded furnace when the same power for the heater is used.

## 4. CONCLUSIONS

Thermal aging is a key technological process in the fabrication of quality aluminum plates, therefore means and methods are needed to adjust the control parameters according to the aging treatment. As with all processes, the prediction of the effect of the specific process parameters adjustment is of concern. Along this line, mathematical and numerical modeling may contribute, add value and provide solutions with minimum costs. More specifically, here we are concerned with the airflow stream and the heating levels that may provide for stable, uniform heating of the aluminum plate batch.

The aging furnace of concern here has a complex structure and monitoring and control scheme. It would exceed the currently available software and hardware resources to approach it as a whole using numerical simulation. Therefore symmetry is assumed and used to define two representatives "cells", which may reduce by five times the computational complexity of the model without interfering with the realistic design, and mathematical modeling and numerical simulation may be used to analyze complex structures and flow patterns.

The fan-driven air stream, the highly complex internal structure, which comprises multiple geometry scales (from narrow channels to vents, deflectors, and larger cavities), suggests that turbulent forced convection may exist, and therefore the Wilcox $k$-$\omega$ a form of the momentum balance is recommended to model it. However, the compressible slightly compressible, or incompressible type of flow is a less obvious decision to start with. To circumvent this difficulty, we use the compressible form to solve the flow – by enabling the last term of the Reynolds averaged Navier-Stokes momentum balance equation (1). Once the airflow is solved we inspect the local Mach number to eventually identify the regions of incompressible airflow inside the furnace. This way, we may infer *a posteriori* that the airflow is mostly turbulent and compressible (as *a posteriori* indicated by local Ma < 0.3) in all parts of the cells. However, for the loaded furnace, there are regions (*e.g.*, the spaces between the aluminum plates) where the flow may be laminar.

The qualitative assessment of the temperature uniformity depends on the airflow inside the furnace and on the power of the heaters that are used in the simulation. Here, the air stream circulation is simplified and modeled by providing the flow velocity at the inlet and the pressure drop at the outlet.

Under steady-state conditions, the temperature inside the furnace is rather constant, uniform, with steep variation (decrease) at the walls. For the input data set that is used in this study, the temperature profiles (Fig. 6) show off that the heating parameters for the aluminum plate batch provide adequate thermal conditions.

## ACKNOWLEDGEMENTS

Part of the cost of the industrial equipment used to obtain the results presented in this work was funded by European Union through Competitiveness Operational Program, Priority Axis 1 Research, Technological Development, and Innovation, within the project "Investments in the R&D Department of ALRO aiming at improving the research infrastructure for the aluminum alloy heat treated plates with high qualification industrial applications", based on the Funding Contract no. 42/05.09.2016. Numerical simulations were conducted in the Laboratory for Multiphysics Modeling at the University POLITEHNICA of Bucharest.

This article is an extension of the paper presented at ***The 39th "Caius Iacob" Conference on Fluid Mechanics and its Technical Applications***, 28 – 29 October 2021, Bucharest, Romania, Virtual Conference, Section 4 – Mathematical Modeling.

## REFERENCES

[1] A. P. Mouritz, *Introduction to Aerospace Materials, Aluminum Alloys for Aircraft Structures*, Woodhead Publishing, pp. 173-201, 2012.

[2] M. Belte, D. Dragulin, A. T. C. Aluvation, Importance of the cooling rate during the heat treatment process of aluminum, *Int. Aluminium J.*, pp. 61-64, 2018.

[3] M. Popa et al., Coupled Fluid Flow and Heat Transfer Analysis of Ageing Heat Furnace, *Light Metals* 2019, Springer International Publishing.

[4] J. Rohde, A. Jeppsson, Literature review of heat treatment simulations with respect to phase transformation, residual stresses, and distortion, *Scand. J. Metall*., **29**, *2*, pp. 47-62, 2010.
[5] J. Mackerle, Finite element analysis and simulation of quenching and other heat treatment processes: A bibliography (1976–2001), *Computational Materials Science*, **27**, *3*, pp. 313-332, 2003.
[6] R. Purushothaman, *Evaluation, and Improvement of Heat Treatment Furnace Model*, Ph.D. thesis, Worcester Polytechnic Institute, June 2008.
[7] E. Hachem*, Stabilized finite element method for heat transfer and turbulent flows inside industrial furnaces,* Mechanics [physics. med-ph]. École Nationale Supérieure des Mines de Paris, PhD thesis, 2009.
[8] D. Saber, H. M. Almalki, Kh. Abd El-Aziz, Design, and building of an automated heat-treatment system for industrial applications, *Alexandria Engineering J.*, **59**, *6*, 2020, pp. 5007-5017, 2020.
[9] * * * Pirometry AMS2750F, *AMS B Finishes Processes and Fluids Committee*, SAE International, 2020-06-29.
[10] D. C. Wilcox, *Turbulence Modeling for CFD*, 2nd ed., DCW Industries, 1998.
[11] D. C. Wilcox, Formulation of the k–ω turbulence model revisited, *AIAA J.*, **46**, pp. 2823-2838, 2008.
[12] W. P. Jones, B. E. Launder, The prediction of laminarization with a two-equation model of turbulence, *International J. of Heat and Mass Transfer*, **15**, pp. 301-314, 1972.
[13] B. E. Launder, B. I. Sharma*,* Application of the energy dissipation model of turbulence to the calculation of flow near a spinning disc*, Letters in Heat and Mass Transfer*, **1**, *2*, pp. 131-138, 1974.
[14] A. Bejan, *Heat Transfer*, Wiley India Edition, 2011.
[15] V. Kriventsev, H. Ohshima, A. Yamaguchi, H. Ninokata, Numerical prediction of secondary flows in complex areas using the concept of local turbulent Reynolds number, *J. of Nuclear Science and Technology*, **40**, *9*, pp. 655–663 (September 2003).
[16] W. Pfeninger, *Transition Experiments in the Inlet Length of Tubes at High Reynolds Numbers, Boundary Layer and Flow Control*, ed. G. V. Lachman, Pergamon, pp. 970–980, 1961.